The Physical and Mechanical Properties of Beta-Nucleated Polypropylene/Montmorillonite Nanocomposites

Yongyut Prachum,[1,2] Roman Helmuth Adam Strauss,[2] Suda Kiatkamjornwong[3]

[1]*Petrochemistry and Polymer Science Graduate Program, Chulalongkorn University, Patumwan, Bangkok 10330, Thailand*
[2]*IRPC Public Company Limited, Rayong, 21000, Thailand*
[3]*Department of Imaging and Printing Technology, Petrochemistry and Polymer Science Graduate Program, Faculty of Science, Chulalongkorn University, Patumwan, Bangkok 10330, Thailand*

Received 18 November 2010; accepted 25 January 2011
DOI 10.1002/app.34209
Published online 20 May 2011 in Wiley Online Library (wileyonlinelibrary.com).

ABSTRACT: Polypropylene (PP) and polypropylene/ polypropylene-*g*-maleic anhydride/ *organomontmorillonite* (PP/PP-*g*-MA/OMMT) nanocomposites were modified with 0.05 to 0.3% (w/w) of the aryl amide β-nucleator to promote the formation of hexagonal crystal modification (β-phase) during melt crystallization. The nonisothermal crystallization behavior of PP, PP/PP-*g*-MA/OMMT and β-nucleated PP/PP-*g*-MA/OMMT nanocomposites were studied by means of differential scanning calorimetry. Structure-property relationships of the PP nanocomposites prepared by melt compounding were mainly focused on the effect and quantity of the aryl amide nucleator. The morphological observations, obtained from scanning electron microscopy, transmission electron microscopy and X-ray diffraction analyses are presented in conjunction with the thermal, rheological, and mechanical properties of these nanocomposites. Chemical interactions in the *nanocomposites* were observed by FT-IR. It was found that the β-crystal modification affected the thermal and mechanical properties of PP and PP/PP-*g*-MA/OMMT nanocomposites, *while the PP/PP-g*-MA/OMMT nanocomposites of the study gained both a higher impact strength (50%) and flexural modulus (30%) compared to that of the neat PP. β-nucleation of the PP/PP-*g*-MA/OMMT nanocomposites provided a slight reduction in density and some 207% improvement in the very low tensile elongation at break at 92% beta nucleation. The crystallization peak temperature (T_{cp}) of the PP/PP-*g*-MA/OMMT nanocomposite was slightly higher (116°C) than the neat PP (113°C), whereas the β-nucleation increased the crystallization temperature of the PP/PP-*g*-MA/OMMT/aryl amide to 128°C, which is of great advantage in a commercial-scale mold processing of the nanocomposites with the resulting lower cycle times. The beta nucleation of PP nanocomposites can thus be optimized to obtain a better balance between thermal and mechanical properties. © 2011 Wiley Periodicals, Inc. J Appl Polym Sci 122: 1066–1076, 2011

Key words: nanocomposites; nucleation; organoclay; spherulites; stiffness

INTRODUCTION

Polypropylene (PP) is a commodity polymer used in a wide range of automotive applications, such as bumpers and interior parts, to packaging applications such as pouches for ready-to-eat meals and other food containers. PP has many desirable properties, such as low density, high thermal stability, and good solvent resistance; however, its modulus relative to engineering polymers, e.g., nylon 6, polycarbonate, etc. is low. This issue is often addressed by adding conventional fillers, e.g., talc or glass fibers.[1] Enhancement of the mechanical and thermal properties of PP can be obtained through PP composites,[1–3] by compounding microfillers (conventional fillers) into the PP matrix. Unfortunately, due to the size or aspect ratio of such fillers, large loadings are required to significantly increase stiffness, which can result in poor processability, lower ductility, and a rough surface finish; and they thus increase the composite product weight or density and cause a drop in impact properties. The use of layered silicates as nanofillers in polymers has gained considerable attention due to the ability to achieve exceptional property enhancements at very low loading levels. Replacing such micro-fillers with layered silicates could potentially alleviate these issues, assuming that good levels of clay dispersion can be achieved. In recent years, a concerted effort has been made to disperse layered silicates in low cost polyolefins, like polypropylene.[1–7] Montmorillonite clay, with its aluminosilicate nanolayers, is a nanofiller which has a much larger aspect ratio and surface area and so can significantly enhance stiffness, thermal properties and scratch resistance levels at a much lower loading ratio, 2 to 7% (w/w), than the conventional microfillers, as long as it is well dispersed and oriented. However, the mechanical properties, which

Correspondence to: S. Kiatkamjornwong (ksuda@chula.ac.th).

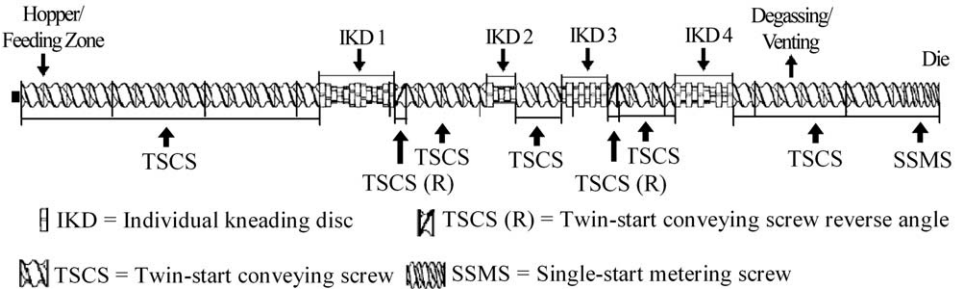

Figure 1 Schematic diagram of screw configuration extrusion using twice direct compounding process.

are related to the toughness or impact strength of PP nanocomposites, are usually reduced in compensation leading to a trade-off of the impact-stiffness balance.

Isotactic polypropylene is known to exhibit four different crystalline forms: alpha, beta, delta, and smectic forms.[8–16] Under normal processing conditions, α-PP is the principle constituent which may be accompanied by a low amount of β-modification. The β-nucleated PP exhibits a much higher impact resistance, but a lower yield strength and elastic modulus, than α-PP.[8,11,12] The formation of the β-form can be promoted in PP by adding various β-nucleators such as quinacridone dye, calcium carbonate, or wollastonite, but the highest selectivity and efficiency were found for calcium salts of pimelic acid[8-11,14-16] and aryl amide compounds.[12,13]

In this work, we report on the preparation of PP nanocomposites with organomontmorillonite (OMMT) in the presence of polypropylene-*g*-maleic anhydride (PP-*g*-MA) as a compatibilizer, to improve stiffness and thermal properties, and simultaneously nucleation with an aryl amide β-nucleator to improve the impact strength of the final nanocomposite for a better mechanical properties and impact-stiffness balance.

EXPERIMENTAL

Materials and composite preparation

Nanocomposites were produced by melt compounding mixtures of a commercial grade homopolymer of propylene (1100NK, IRPC Public Co. Ltd., Rayong, Thailand, MFI at 230°C/2.16 kg = 12 g/10 min, MW = 300,000), polypropylene-*graft*-maleic anhydride (PP-*g*-MA, Crompton, Smithfield, PA, MFI at 190°C/2.16 kg = 110 g/10 min, MW = 120,000, MA content = 1.0% (w/w)) used as a compatibilizer, and an organoclay (organomontmorillonite, OMMT). The OMMT used in this study was Nanofil SE3000, purchased from Süd Chemie, Moos-burg, Germany. According to the supplier, the original clay was Na^+-MMT, which was intercalated with 35% by weight of distearyldimethylammonium chloride salt. A master batch of PP/PP-*g*-MA/OMMT at a ratio of 40/30/30 (%, w/w/w) and another master batch of PP/aryl amide nucleator (aryl amide compound, Xiang Yang Co., Anhui, China) at a ratio of 95/5 (%, w/w) were prepared by a twin screw corotating extruder (LTE 26-40, LAB TECH Engineering Co., Ltd., Bangkok, Thailand) before they were let down with the bulk PP in the same extruder. The extruder had a 26-mm diameter screw and an $L/D = 40$. The designed screw configuration is illustrated in Figure 1 with the assemble of Twin-start conveying screw (TSCS), Twin-start conveying screw reverse angle (TSCS (R)), individual kneading disc (IKD) and single-start metering screw (SSMS). Before melting, all the components were dried at 90°C for 10 h. The PP, PP-*g*-MA, OMMT, and aryl amide (PP/PP-*g*-MA/OMMT/aryl amide compounds) were melt mixed with the ratios indicated in Table I. Neat PP, a master batch of PP/PP-*g*-MA/OMMT at a ratio of 40/30/30 (%, w/w/w) and a master batch of PP/aryl amide nucleator at a ratio of 95/5 (%, w/w), were dry blended by tumble mixing and fed simultaneously into the twin screw corotating extruder using a temperature profile of 160 to 195°C (from the hopper to the die), at a feed rate of 10 kg/h and a screw speed of 250 rpm. The extruded strands were water cooled and pelletized with a strand cutter (LZ-120/VS, LAB TECH Engineering Co. Ltd., Bangkok, Thailand). These pellet samples were dried at 90°C for 10 h and then molded to form test specimens for mechanical testing by injection molding (Arburg allrounder® 270M, Arburg Co., Lossburg, Germany).

Morphology characterization

The mixture of distearyldimethylammonium chloride modified MMT, maleic anhydride grafted polypropylene, and polypropylene was melt processed to achieve polymer clay nanocomposites. The structures of PP nanocomposites were studied using X-ray diffraction (XRD),[4,17] scanning electron microscopy (SEM),[18] and transmission electron microscopy (TEM), as outlined below.

TABLE I
The Formulation of PP/PP-*g*-MA/OMMT/Aryl Amide Nanocomposites

Recipe No.	PP/PP-*g*-MA/OMMT/ aryl amide (% (w/w))	Weight fraction (% (w/w))			
		PP	PP-*g*-MA	OMMT	Aryl amide
1	100/0/0/0 (Neat PP)	100	0	0	0
2	99.9/0/0/0.1	99.9	0	0	0.1
3	99.7/0/0/0.3	99.7	0	0	0.3
4	95/5/0/0	95	5	0	0
5	95/0/5/0	95	0	5	0
6	90/5/5/0	90	5	5	0
7	89.95/5/5/0.05	89.95	5	5	0.05
8	89.9/5/5/0.1	89.9	5	5	0.1
9	89.7/5/5/0.3	89.7	5	5	0.3

X-ray diffractometry (XRD)

The diffraction patterns and crystallinity were analyzed with the XRD (TTRAX III, Rigaku Corp., Tokyo, Japan) using Ni-filtered Cu Kα radiation, having a wavelength of 0.154 nm, and operated at 50 kV and 300 mA. The diffraction spectra were recorded over a 2θ range of 1 to 30° in steps of 0.02°/s. The neat PP, β-nucleated PP, OMMT, PP nanocomposites, and β-nucleated PP nanocomposites samples were compressed in a hot-press compression mold (LAB TECH Engineering Co., Ltd., Bangkok, Thailand) at 170°C for five min to produce 2-mm thick sheets with smooth and flat surfaces. The XRD analysis of all specimens was performed at room temperature. The basal spacing of the montmorillonite galleries and the crystalline form were calculated from the XRD patterns using Bragg's equation, $n\lambda = 2d\sin\theta$, where d is the interplanar distance of the (001) reflection plane, θ is the diffraction angle, λ is the wavelength.

Transmission electron microscopy (TEM)

TEM observations were carried out to examine the dispersion morphology of montmorillonite in both β-nucleated nanocomposite and nanocomposites. Ultrathin sections (60–80 nm) for transmission electron microscopy (TEM-2010F, JEOL Corp., Tokyo, Japan) analysis were microtomed by an Ultramicrotome having a cryo mode (RMC MTX model, Research Manufacturing Co., Tucson, AZ) from the central and skin regions of a tensile bar at −90°C. Cuts were made perpendicularly to the flow direction of the injection molded specimens from the middle of tensile bar and halfway between the top and bottom surfaces. The thin slices were placed on 300 mesh copper grids and then analyzed by TEM with LaB6 filament operating at 80 kV.

Scanning electron microscopy (SEM)

For SEM investigation, the tensile bar specimens for the neat PP, 90/5/5/0, 99.7/0/0/0.3 and 89.7/5/5/0.3 nanocomposites were fractured in liquid nitrogen at the direction perpendicular to the injection flow direction, and then gold-coated and observed under an acceleration voltage of 15 kV with an SEM (JSM-5900 LV, JEOL Corp., Tokyo, Japan). Additionally, the same fractured specimens were etched as reported in Olley et al.,[18] then gold-coated and analyzed.

Rheological properties by small amplitude oscillatory shear analysis

A cone and plate rheometer (Physica MCR 301, Anton Paar Co., Graz, Austria) was used to measure the rheological characteristics of the neat PP and PP-based nanocomposites according to Table I, using the parallel plate fixture (25 mm plate diameter, 1.7 mm gap). All the rheological measurements were carried out at a constant temperature of 220°C under nitrogen gas. Strain sweep tests were carried out for each sample to ensure that the strain used was within the linear viscoelastic range. Frequency sweep tests were made over a range of 0.01 to 100 rad/s at 5% strain, which is within the linear region for each sample. Specimens for rheological testing, as 25 mm diameter discs of 2 mm thickness, were molded in a hot-press (LAB TECH Engineering Co., Ltd., Bangkok, Thailand) at 170°C for 5 min.

Thermal analysis

DSC measurements were made on Mettler Toledo thermal systems (DSC1, Mettler Toledo International Inc., Greifensee, Switzerland) under nitrogen atmosphere with 10°C/min heating and cooling rates. Each sample for analysis weighed 10 ± 0.01 mg. The samples were heated from 30 to 200°C, held at 200°C for 5 min to erase the thermal history, and then cooled to 30°C, followed by reheating to 200°C for the second scan. The crystallization and melting parameters were recorded from the cooling and reheating scans. The percentages and crystallinity of β-phase Φ_β were calculated from the crystallinities of

the α-phase and β-phase according to eqs. (1) and (2) below, as previously reported[15,16]:

$$X_i = \frac{\Delta H_i}{\Delta H_i^{\theta}} * 100 \quad (1)$$

$$\Phi_{\beta}(\%) = \frac{X_{\beta}}{X_{\alpha} + X_{\beta}} * 100 \quad (2)$$

where X_i is the percentage crystallinity of the α-phase or β-phase, calculated according to eq. (1). The term ΔH_i is the specific heat of fusion of either the α-form or the β-form and ΔH_i^{θ} is the standard heat of fusion for 100% α-and β-crystals of *i*PP, being 178 and 170 J/g, respectively.[15,16] The total crystallinity is the sum of the crystallinity from the alpha and the beta portions. The crystallization behavior of polymer nanocomposites was studied using nonisothermal crystallization tests at cooling rates of 10°C/min.

To characterize the effect of nanoclay particles on the nature and size of spherulites, a high temperature stage (TH600, Linkam Scientific Instruments Ltd., Surrey, UK) equipped with a Nikon polarizing light microscope (Nikon, Nikon Corp., Tokyo, Japan) was used. The extruded pellet sample was compressed to form a thin film (50 μm) at 170°C by compression molding. The samples were isothermally crystallized at 135°C after erasing the thermal history at 200°C for 5 min and micrographs (400× magnification) were taken *in situ* using a Nikon digital camera attached to the microscope.

Fourier Transform-infrared spectroscopy (FT-IR)

FTIR was used to investigate the interaction between the PP, PP-*g*-MA, OMMT, and aryl amide β-nucleator.[19] The PP nanocomposite was compression molded at 170°C to produce 50 μm thin film samples. The FT-IR scans were performed at an ambient temperature in the range of 400 to 4,000 cm^{-1} on a Bruker FT-IR spectrometer (Vertex 70, Bruker Optik GmbH, Ettlingen, Germany).

Mechanical properties

The polymer specimens (64 × 12.7 × 3.2 mm) for Izod impact strength (notched) properties were prepared following ASTM D4101 and analyzed by Pendulum impact tester (Zwick GmbH and Co. KG, Ulm, Germany) according to ASTM D256. Flexural modulus and flexural strength were obtained under 3-point loading conditions at room temperature. Test specimens of 128 × 12.7 × 3.2 mm were prepared following ASTM D4101 and tested by Instron 4465 universal testing machine (Instron Co., Norwood, MA) according to ASTM D790. The dumbbell specimens (128 × 12.7 × 3.2 mm) for tensile properties were prepared following ASTM D4101 and tested by Instron 4465 universal testing machine (Instron Co., Norwood, MA) according to ASTM D638. For the heat deflection temperature (HDT), the specimens were also prepared based on ASTM D4101 and tested by an HDT Vicat tester (Yasuda 148, Yasuda Seiki Seisakusho, Tokyo, Japan) according to ASTM D648.

Density

Polymer specimens of 12.7 × 12.7 × 3.2 mm were prepared by following ASTM D4101 and tested by Mettler Toledo Balance (AT201, Mettler Toledo International Inc., Greifensee, Switzerland) according to ASTM D792 method B.

RESULTS AND DISCUSSION

The effect of β-nucleation of PP/PP-*g*-MA/OMMT nanocomposites

Morphology

The PP/PP-*g*-MA/OMMT nanocomposites characterized by the XRD techniques indicate that the grafted PP with polar groups can be intercalated into the organoclay, expanding the galleries and inducing the incorporation of polypropylene.[20] The series of X-ray diffraction spectra of OMMT, PP/PP-*g*-MA/OMMT nanocomposites, and PP/PP-*g*-MA/OMMT nanocomposites with various amounts of aryl amide nucleator are summarized in Table II with representative spectra shown in Figure 2. The monoclinic phase (alpha phase) of the neat PP and the PP/PP-*g*-MA/OMMT nanocomposites was identified at the (110), (040), (130), (111), and (041) crystallographic planes corresponding to the diffraction angles 2θ of 14.1°, 16.8°, 18.5°, 21.1°, and 21.8°, respectively. The neat PP and 90/5/5/0 (PP/PP-*g*-MA/OMMT/aryl amide) nanocomposite did not produce any detectable hexagonal (β-phase) form crystal structures. The hexagonal crystal forms in neat PP and PP nanocomposites were only observed in the presence of the aryl amide nucleator in nanocomposite samples comprised of 99.9/0/0/0.1, 89.95/5/5/0.05, 89.9/5/5/0.1, and 89.7/5/5/0.3 (PP/PP-*g*-MA/OMMT/aryl amide). The main diffraction characteristics of β-nucleated PP and PP nanocomposites were clearly observed at 2θ = 16.0° which was associated with the (300) planes. The β-phase content in crystalline *i*PP, the so-called k_{β}, was calculated using the formula proposed by Turner-Jones et al.[21] in eq. (3) as follows:

$$k_{\beta} = \frac{H_{\beta 1}}{H_{\beta 1} + (H_{\alpha 1} + H_{\alpha 2} + H_{\alpha 3})} \quad (3)$$

where $H_{\alpha 1}$, $H_{\alpha 2}$, and $H_{\alpha 3}$ are the intensities of α-diffraction peaks corresponding to 2θ = 14.1°, 16.8°, and 18.5°, respectively, while $H_{\beta 1}$ is the intensity of

TABLE II
XRD Data and Density of the Neat PP and PP/PP-*g*-MA/OMMT Nanocomposites Formulated with Various Amounts of Aryl Amide Nucleator

Formulation	2θ of (001) plane (°)	d-spacing at (001) plane (nm)	Intensity at (001) plane	k_β	*Density (kg/m^3)
Neat PP	None	None	None	0.01	904.12 ± 0.41
99.9/0/0/0.1	None	None	None	0.93	901.34 ± 0.28
OMMT	2.42	3.65	16,356	0.00	[a]
95/0/5/0	2.40	3.68	16,494	0.00	[a]
90/5/5/0	None	None	None	0.00	921.29 ± 0.06
89.95/5/5/0.05	2.38	3.71	6,587	0.49	[a]
89.9/5/5/0.1	2.28	3.87	7,526	0.92	[a]
89.7/5/5/0.3	2.26	3.9	11,980	0.92	919.01 ± 0.44

The results are the average of three specimens.
[a] Was not determined.

β-diffraction peak corresponding to the angle 2θ = 16.0°. The fraction of the hexagonal form can be expressed by the k_β value from eq. (3).

The effect of addition of the aryl amide β-nucleator on neat PP and the dispersion of OMMT in PP/PP-*g*-MA/OMMT/aryl amide nanocomposites were also observed via XRD in Figure 2(a–f) and TEM in Figure 3. Figure 2(b) shows the XRD spectrum of the neat PP in which only alpha crystallinity was found because no beta crystallinity peaks at 2θ = 16.0° occurred. When adding 0.1% of beta nucleator into neat PP, the beta crystallinity peak was mainly generated at 2θ = 16.0° as shown in Figure 2(a) with a k_β value of 0.93 (Table II). The interlayer spacing of pristine OMMT, as shown in an inset in Figure 2 and Table II, is 3.65 nm at 2θ = 2.42° with high intensity before compounding.

For the compatibilizer-free PP/OMMT nanocomposites (95/0/5/0), the interlayer spacing of OMMT is 3.68 nm at 2θ = 2.40° with high intensity which is similar to that from the pristine OMMT as shown in Table II, suggesting a poor or nondispersion of OMMT. In the compatibilized system of composition 90/5/5/0 in Figure 2(f), X-diffraction peaks in the 2θ range of 1 to 5° are either broadened with very low intensity or markedly disappeared. The interlayer spacing of OMMT of those systems could not be determined, suggesting a highly disordered, partially exfoliated and exfoliated OMMT.[4] This implies that intercalation of PP chains into the intergalleries of OMMT and some exfoliation of OMMT layers had taken place. The addition of 0.05% (w/w) aryl amide, labeled as 89.95/5/5/0.05 PP nanocomposite in Figure 2(e), induced the beta nucleation with a k_β value of 0.49 (Table II) whereas the characteristic X-ray diffraction pattern showed that the interlayer spacing of OMMT is 3.71 nm at 2θ of 2.38° with low intensity, suggesting a rather high disordered and only intercalated OMMT. This was different from that observed with the aryl amide free 90/5/5/0 nanocomposite in Figure 2(f), indicating a poorer level of dispersion of the OMMT. At the level of 0.1% (w/w) of the nucleator [Fig. 2(d)], the beta form increased to produce the k_β value of 0.92 (Table II), while the diffraction peaks in the 2θ range of 1 to 5° were still observed with a low intensity and shifted to the lower angle at 2θ of 2.28°. This means that the interlayer spacing of OMMT was extended to 3.87 nm, suggesting a rather high disordered and only intercalated OMMT, which was different from that observed with the aryl amide free 90/5/5/0 nanocomposite in Figure 2(f), indicating also a poorer level dispersion of the OMMT. However, from the results of TEM micrographs in Figure 3, some partially exfoliated and intercalated OMMT were obtained in both 89.9/5/5/0.1 and 90/5/5/0 nanocomposites as shown in Figure 3(a,b), respectively, indicating that both nanocomposites have a little different dispersion level of OMMT. From the

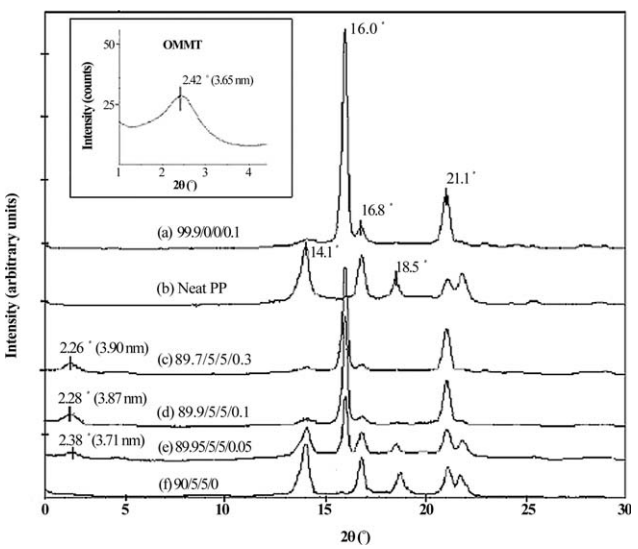

Figure 2 XRD patterns of neat PP and PP/PP-*g*-MA/OMMT/aryl amide nanocomposites: (a) 99.9/0/0/0.1; (b) 100/0/0/0 (neat PP); (c) 89.7/5/5/0.3; (d) 89.9/5/5/0.1; (e) 89.95/5/5/0.05; and (f), 90/5/5/0.

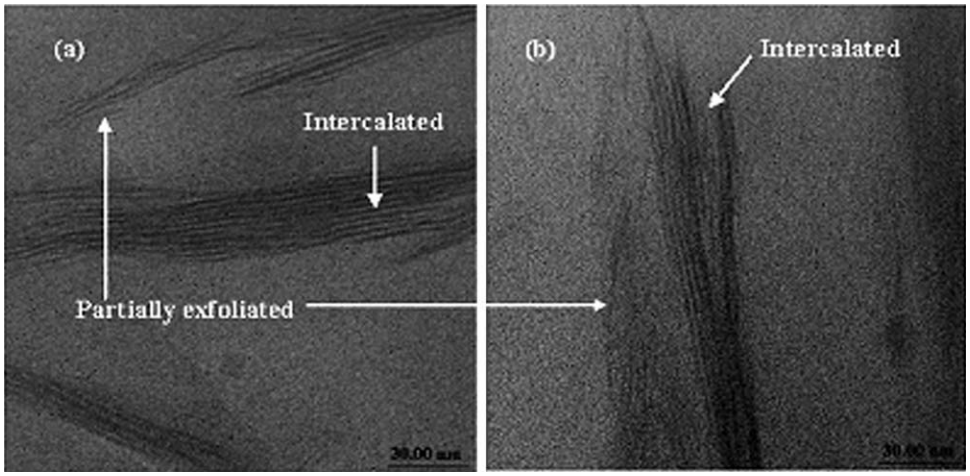

Figure 3 TEM micrographs of the composites showing the intercalated and partially exfoliated layers: (a) 89.9/5/5/0.1; and (b) 90/5/5/0, at 100,000 magnifications.

results of both XRD and TEM techniques, we can conclude that a dispersion level of OMMT in 90/5/5/0 nanocomposite is better than both 89.95/5/5/0.05 and 89.9/5/5/0.1 nanocomposites. At the level of 0.3% (w/w) of the nucleator shown in Figure 2(c), the beta form gives the same k_β value of 0.92 (Table II). The diffraction peak was observed at the lower angle at 2θ of 2.26° with a high intensity (sharp peak). This means that the interlayer spacing of OMMT was widened to 3.90 nm, suggesting the intercalated or flocculated OMMT and the lowest disordered level compared with the silicate layers in 90/5/5/0, 89.95/5/5/0.05 and 89.9/5/5/0.1 nanocomposites. Based on these results, however, the effect of β-nucleation on the dispersion of OMMT in PP nanocomposite cannot be clearly explained.

Density. Table II also lists the densities of samples where a slightly lower density of the β-nucleated samples was found compared with the α-form, a result of which is in good agreement with Michler and Balta-Calleja.[9] While the density of nanocomposites containing 5% (w/w) nanoclay composites was 1.9% higher than that of neat PP, the β-nucleation can partially compensate for the negative effect of higher part weights, because the density of the corresponding β-nucleated 89.7/5/5/0.3 PP nanocomposites increased only by about 1.6%, that is, a 15% reduction of the level of increased density. The representative SEM micrographs shown in Figure 4 reveal the etched fractured surfaces of the neat PP and nanocomposites without and with 0.3% of the beta nucleator. The α-form PP and PP nanocomposites (90/5/5/0) in Figure 4(a,b) present a cross-hatched structure, smooth fractured surface, and fine porosity. The sheaf-like lamellar structure containing radial arrays of the parallel stacked lamellae of β-nucleated PP[9,10] in 99.7/0/0/0.3 nanocomposite of Figure 4(c), and a rough fractured surface with large pores in 89.7/5/5/0.3 nanocomposite of Figure 4(d) were observed from the etched fractured surface tensile specimens. The results exhibit that β-nucleated PP and β-nucleated nanocomposite are of higher porosity which imposes effects on the nanocomposite density.

The rheological properties of neat PP, PP/PP-*g*-MA blend, PP/PP-*g*-MA/OMMT, and β-nucleated PP/PP-*g*-MA/OMMT nanocomposites

The rheological properties of the nanocomposites are sensitive to surface characteristics and the level of dispersion. Therefore, melt rheology can be utilized as a powerful tool for characterizing the state of dispersion, intercalation, and exfoliation of clay nanocomposites.[4,6,22,23] The storage modulus G', and complex viscosity η* were each measured as a function of the oscillation frequency for the PP/PP-*g*-MA melt blend. No specific effects on G', and η* were observed between the neat PP and the 95/5/0/0 blend, indicating a good miscibility between PP and PP-*g*-MA (Fig. 5). The rheological behavior of this binary blend, which corresponds to the weight ratios present in the PP/PP-*g*-MA/OMMT nanocomposites, is therefore used as the reference matrix behavior. The values of G', and η* as a function of the oscillating frequency for the neat PP and the nanocomposites with different β-nucleator loadings are summarized in Figure 8. At low frequencies (<1 rad/s), G', and η* all increased significantly when OMMT and PP-*g*-MA were added in 90/5/5/0 nanocomposite, which is associated with a high PP intercalation and partial exfoliation of the OMMT in the PP matrix. Referring to Wang et al.,[24] Solomon et al.,[22] and Kim et al.,[7] the increase in storage modulus at low frequency can be explained by the existence of a percolated network microstructure. By further adding 0.05, 0.1 and 0.3% (w/w) of the β-nucleator aryl amide to these PP nanocomposites,

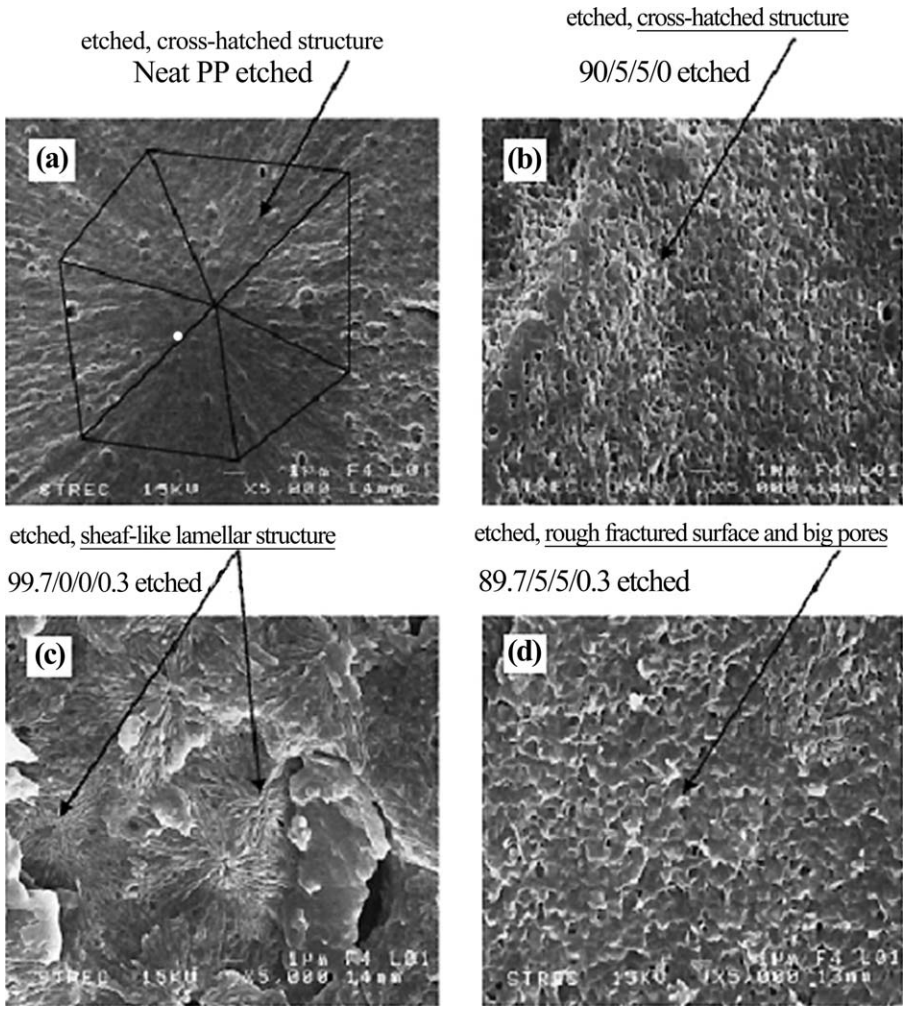

Figure 4 Scanning electron micrographs of the etched, fractured impact surface of (a) neat PP and PP/PP-*g*-MA/OMMT/aryl amide nanocomposites: (b) 90/5/5/0; (c) 99.7/0/0/0.3; and (d) 89.7/5/5/03.

slight decreases in G' and η^* were observed, confirming a little poorer dispersion of OMMT compared with the β-nucleated free nanocomposite (90/5/5/0). However, the effect of β-nucleating on the dispersion of OMMT cannot be explained simply based on the results obtained from this study.

Thermal properties

The DSC measurements revealed the melting and crystallization characteristics of the nucleated and non-nucleated PP homopolymer (neat PP) and PP nanocomposites under nonisothermal conditions as shown in Table III, Figures 6 and 7. The crystallization temperature (T_c) of PP/PP-*g*-MA/OMMT was slightly higher than that of the neat PP. These results agree well with that of Wang et al.[24] and indicate that OMMT acts as an α-nucleating agent in the nanocomposites. The PP and PP nanocomposites containing 0.05 to 0.3% (w/w) aryl amide nucleator crystallized are essentially a β-modification structure as shown by the β-melting peaks (Table III). In the β-modification of PP and PP nanocomposites, the α-and β-melting peaks are practically identical. There is a distinctive β-fusion peak at 154°C and α-fusion at 169°C. The DSC thermograms can be used to evaluate the performance of the aryl amide nucleator in both PP and the PP/PP-*g*-MA/OMMT nanocomposites, as shown in Table III. The degrees of crytallinity and the percentage of α-and β-fractions were determined from the respective fusion peaks of the DSC thermogram according to eqs. (1) and (2) and are summarized in Table III. Addition of 0.1 to 0.3% (w/w) of the β-nucleator induced very high β-modification levels in the neat PP and PP nanocomposites, up to 92% ($k_\beta = 0.92$) of the total crystallinity, and significantly increased the crystallization temperature of both the neat PP and the PP/PP-*g*-MA/OMMT nanocomposites. Representative crystallization thermograms of the PP, PP/PP-*g*-MA/OMMT, and β-nucleated PP/PP-*g*-MA/OMMT nanocomposites are shown in Figure 6 for a cooling rate of 10°C/min. From these thermograms, the

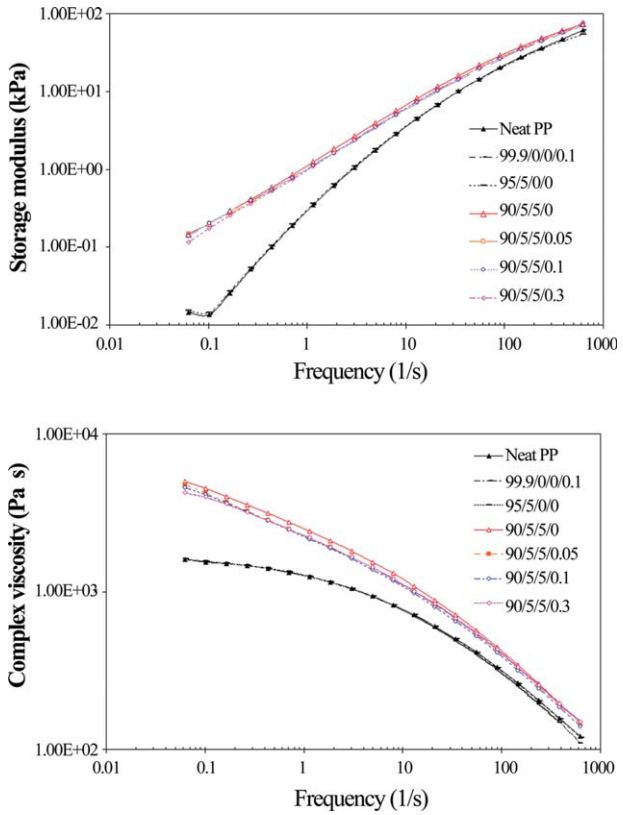

Figure 5 Rheological properties of (a) storage modulus; and (b) complex viscosity of PP, PP/PP-*g*-MA and PP/PP-*g*-MA/OMMT nanocomposites with various loadings of aryl amide nucleator determined by Cone and Plate Rheometer. [Color figure can be viewed in the online issue, which is available at wileyonlinelibrary.com.]

crystallization onset temperature (T_{co}) and crystallization peak temperature (T_{cp}), and the heat evolved during crystallization (ΔH_c) were determined and are summarized in Table III. The presence of the β-nucleator leads to a significant increase in T_{cp} and T_{co} increases with increasing β-nucleator content. At a cooling rate of 10°C/min, the crystallization peak temperature (Fig. 7) for the PP/PP-*g*-MA/OMMT (90/5/5/0) nanocomposite is 116°C compared with 113°C for the neat PP. This shows that OMMT acts as a high performance nucleating agent because the addition of PP-*g*-MA alone to PP reduces the rate of crystallization significantly,[5] while for the 0.05, 0.1, and 0.3% (w/w) β-nucleated nanocomposites (89.95/5/5/0.05, 89.9/5/5/0.1, 89.7/5/5/0.3), T_{cp} increases to 123, 124, and 128°C, respectively. In the PP/PP-*g*-MA/OMMT nanocomposites with the efficient aryl amide β-nucleator, the crystallization temperature increased by up to 13°C, therefore, cycle time and energy consumption for industrial PP nanocomposite processing are significantly shortened.

Aryl amide is a very effective nucleating agent to increase the number of β-crystals and the rate of crystallization in PP/PP-*g*-MA/OMMT nanocomposites by the formation of more and smaller spherulites in a heterogeneous nucleation process. A nucleation effect is also confirmed by examination of the polarized light microscopic images, as shown in Figure 8(a,b). Figure 8(a) illustrates the large-sized spherulites (about 100 μm) of the neat PP which contains more than 95% of the alpha form whereas in Figure 8(b), the β-nucleated PP shows two size ranges of β-spherulites, i.e., about 10 μm small spherulites in some areas, and approximately 100 μm large spherulites with voids at the center in other areas. For the β-nucleated free nanocomposite, PP/PP-*g*-MA/OMMT (90/5/5/0) in Figure 8(c), the spherulite size of alpha form is reduced to 50 to 80 μm, presumably that OMMT acts as a nucleating agent. For the β-nucleated nanocomposite (89.9/5/5/0.1) in Figure 8(d), the spherulite size is reduced to 10 to 25 μm. This is caused by the very effective nucleating agent of aryl amide to increase the number of β-crystals and the rate of crystallization in PP/PP-*g*-MA/OMMT nanocomposites to generate more and smaller spherulites in a heterogeneous nucleation process.

Mechanical properties

The mechanical properties of the neat PP, β-PP, PP/PP-*g*-MA (95/5/0/0), PP/OMMT (95/0/5/0), and PP/PP-*g*-MA/OMMT nanocomposites with various amounts of β-nucleator are summarized in Table IV.

TABLE III
Thermal Properties of PP and PP/PP-*g*-MA/OMMT Nanocomposites Formulated with Various Amounts of Aryl Amide Nucleator

Formulation	ΔH_α (J/g)	X_α	$T_{m-\alpha}$ (°C)	ΔH_β (J/g)	X_β	$T_{m-\beta}$ (°C)	ΔH_c (J/g)	T_{co} (°C)	T_{cp} (°C)	Total crystallinity[a]	Φ_β (%)
Neat PP	89.5	0.5	165	0.00	0.00	None	97.6	118	113	0.50	0
90/5/5/0	83.7	0.47	166	0.00	0.00	None	94.5	121	116	0.47	0
99.9/0/0/0.1	9.8	0.06	169	79.3	0.47	154	97.6	130	127	0.52	89
89.95/5/5/0.05	56.9	0.32	167	33.0	0.19	154	96.9	127	123	0.51	38
98.9/5/5/0.1	12.9	0.07	169	70.3	0.41	154	92.4	129	124	0.49	85
89.7/5/5/0.3	6.9	0.04	169	78.4	0.46	154	88.9	132	128	0.50	92

Based on the DSC curves recorded at the cooling and heating rates from 10°C/min.
[a] Total crystallinity = alpha crytallinity and beta crytallinity. ND = cannot be determined.

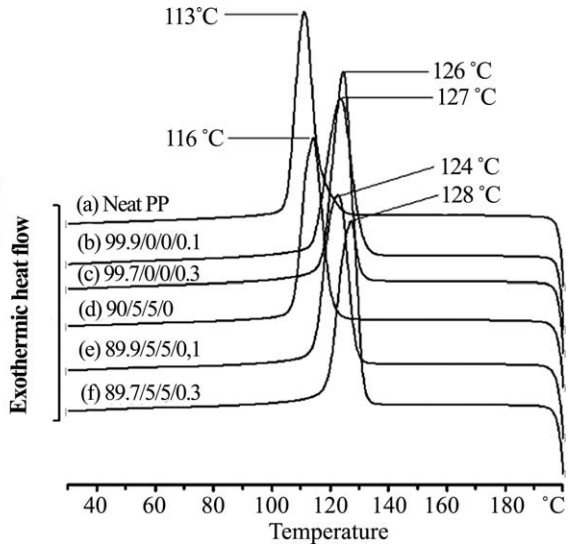

Figure 6 DSC thermograms and crystallization temperatures of (a) neat PP and PP/PP-*g*-MA/OMMT/aryl amide nanocomposites: (b) 99.9/0/0/0.1; (c) 99.7/0/0/0.3; (d) 90/5/5/0 (e) 89.9/5/5/0.1; and (f) 89.7/5/5/0.3 recorded by the DSC curves with a scanning rate of 10°C/min from 25 to 200°C.

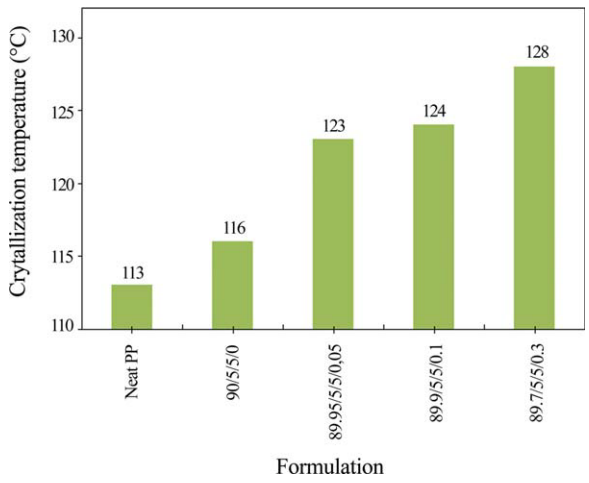

Figure 7 Effect of nanocomposite formulations on crystallization temperature at a cooling rate of 10°/min. [Color figure can be viewed in the online issue, which is available at wileyonlinelibrary.com.]

The morphology of thermoplastic polyolefins-based nanocomposites has shown to influence their mechanical properties.[1,7] Here, the flexural modulus (1,332 ± 20 MPa) of β-nucleated PP (99.9/0/0/0.1, $k_\beta = 0.93$) was slightly lower than that of the neat PP (1,413 ± 17 MPa), while the elongation at break was not changed and Izod impact strength was drastically improved by some 136% from 28.6 ± 0.2 J/m in the neat PP to 67.6 ± 2.0 J/m in 99.9/0/0/0.1, β-nucleated PP. The flexural modulus and Izod impact strength of PP/PP-*g*-MA (95/5/0/0) blend are higher than that for the neat PP by approximately 12 and 26%, respectively. The flexural modulus and Izod impact strength of the compatibilizer free PP/OMMT nanocomposites (95/0/5/0) are higher than that for the neat PP by approximately 23 and 34%, respectively. These results relate to a stronger interaction between clay and PP. A stronger nucleation of the clay leading to a significant reduction in spherulite size is responsible for increasing in toughness on reinforcement of PP which were explained by Deshmane et al.[19] Besides, impact strength improvement could be also attributed to the size reduction of clay tactoids.[25] In the PP/PP-*g*-MA/OMMT nanocomposites (90/5/5/0), the flexural modulus and Izod impact strength are much higher than that for the neat PP by approximately 30 and 50%, respectively. These results indicate the synergistic effect of PP-*g*-MA and OMMT relates to a good dispersion of OMMT (a highly disordered and partially exfoliated OMMT), which confirms a good compatibilization and interaction among the OMMT, PP-*g*-MA, and PP matrix; while a very low elongation at break for these reinforced nanocomposites were obtained, as expected. The addition of 0.05% (w/w) of the β-nucleator to the PP/PP-*g*-MA/OMMT nanocomposites induced the β-form at the k_β value of 0.49 (Table II), and the elongation at break was greatly improved by about 70%, while Izod impact strength was slightly higher and flexural modulus slightly lower. Besides the amount and the type of crystallinity, a little poorer dispersion of OMMT (a rather high disordered and only intercalated OMMT) compared with PP/PP-*g*-MA/OMMT nanocomposites

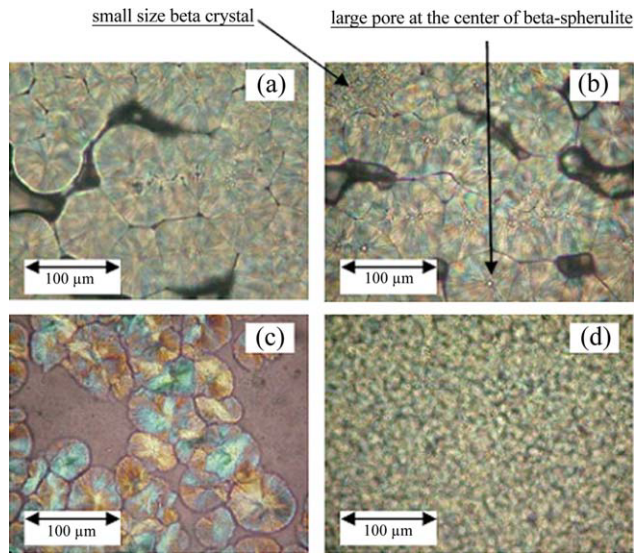

Figure 8 Optical micrographs of the neat PP, and PP/PP-*g*-MA/OMMT nanocomposites under an isothermal condition at 135°C for (a) Neat PP (>95% α-form) 20 min at 135°C, spherulite size 70 to 100 µm; (b) 99.9/0/0/0.1 (92% β-form), 20 min at 135°C 10 µm, spherulite size 100 µm; (c) 90/5/5/0, 20 min at 135°C, spherulite size 50 to 80 µm; (d) 89.9/5/5/0.1, 10 min at 135°C, spherulite size 10 to 25 µm. [Color figure can be viewed in the online issue, which is available at wileyonlinelibrary.com.]

TABLE IV
Mechanical Properties of PP/PP-*g*-MA/OMMT Nanocomposites Formulated with Various Amounts of the Beta-Nucleating Agent

Formulation	k_β	Flexural modulus (MPa)	Izod impact strength at 23°C (J/M)	Elongation at break (%)	Heat deflection temperature (HDT) (°C)
100/0/0/0 (Neat PP)	0.00	1,413 ±17	28.6 ± 0.2	1,087 ± 23	105 ± 1
99.9/0/0/0.1	0.93	1,332 ± 20	67.6 ± 2.0	1,063 ± 103	120 ± 1
95/5/0/0	0.00	1,588 ± 12	36.1 ± 1.5	230 ± 20	119 ± 1
95/0/5/0	0.00	1,736 ± 21	38.4 ± 1.8	132 ± 15	123 ± 1
90/5/5/0	0.00	1,825 ± 6	43.0 ± 1.8	54 ± 5	127 ± 1
89.95/5/5/0.05	0.49	1,777 ± 14	45.8 ± 1.7	91 ± 4	126 ± 1
89.9/5/5/0.1	0.92	1,821 ± 22	40.3 ± 2.0	50 ± 7	126 ± 0
89.7/5/5/0.3	0.92	1,747 ± 9	35.3 ± 1.0	166 ± 31	128 ± 1

The number of repeat for HDT is three while the other is five.

(90/5/5/0) can also affect the mechanical properties. Likewise, the addition of 0.10% (w/w) of the β-nucleator to the PP/PP-*g*-MA/OMMT nanocomposites induced the β-form to give the k_β value of 0.92 (Table II), the elongation at break and flexural modulus were similar but the Izod impact strength was slightly higher. This result indicates a bit poorer dispersion of OMMT (a rather high disordered, intercalated and some partially exfoliated OMMT) compared with that of PP/PP-*g*-MA/OMMT nanocomposite (90/5/5/0). The addition of 0.30% (w/w) of the β-nucleator to the PP/PP-*g*-MA/OMMT nanocomposites also induced the β-form to give the k_β value of 0.92 (Table II), the elongation at break was significantly improved, by up to 207%, whereas the flexural modulus and Izod impact strength were both somewhat reduced by about 4 and 18%, respectively. This is resulted from a poorer dispersion of OMMT (a low disordered and intercalated or flocculated OMMT) and the poorer flexural modulus of β-crystallinity in the β-nucleated nanocomposite compared with that of PP/PP-*g*-MA/OMMT nanocomposite (90/5/5/0). Finally, while the heat deflection temperature (HDT) of the β-nucleated PP is significantly higher than that of the α-PP, the amount of β-nucleation did not appear to affect the HDT of the PP/PP-*g*-MA/OMMT nanocomposites.

Structure characterization and possible interaction

To observe any changes and chemical interactions in the PP/PP-*g*-MA/OMMT nanocomposites, Fourier Transform-infrared spectroscopy (FT-IR) was

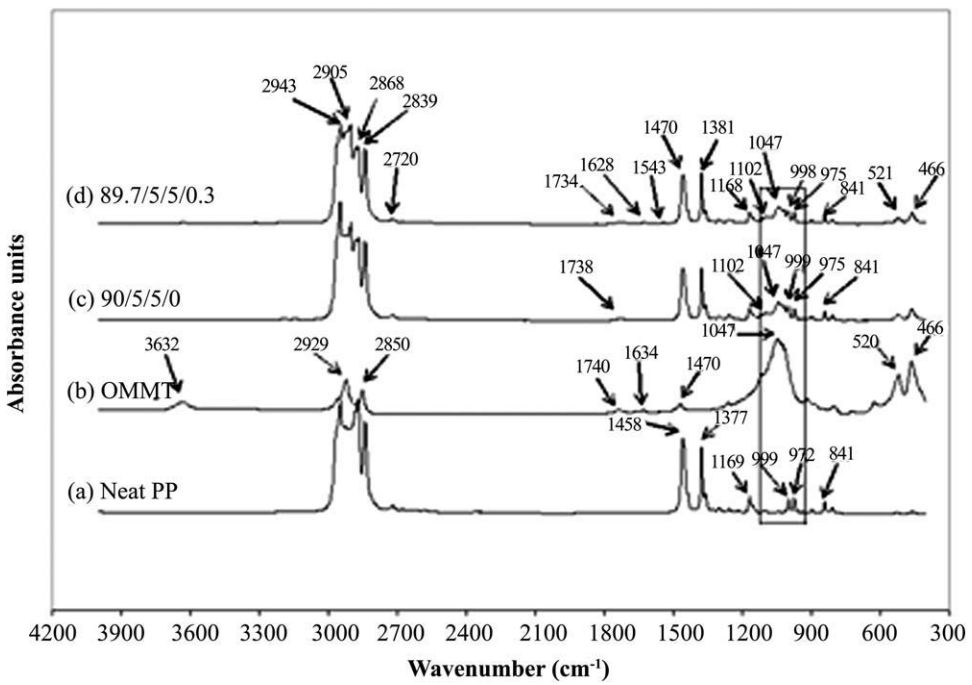

Figure 9 Fourier transformed-infrared spectroscopic spectra of: (a) neat PP; (b) montmorillonite; PP/PP-*g*-MA/OMMT/aryl amide nanocomposites: (c) 90/5/5/0; and (d) 89.7/5/5/0.3.

applied.[19,26] Representative FT-IR spectra of the clay, the neat polymer, PP/PP-*g*-MA/OMMT, and PP/PP-*g*-MA/OMMT/aryl amide nanocomposites are presented in Figure 9(a–d). For the neat PP in Figure 9(a), 1,458 cm^{-1} for δ_{as} (CH_3); 1,377 for δ_s (CH_3), and 1,169 cm^{-1} for CH_2 out of plane wagging; 999, 972, 841 cm^{-1} for tertiary methyl stretch deformations. The IR spectrum for OMMT in Figure 9(b) shows a peak at 1,470 cm^{-1} which is associated with methylene (CH_2) wagging deformation of alkyl ammonium surface modified clay, 1,047 cm^{-1} for ν (Si-O) out-of-plane, 520 cm^{-1} for Si-O stretching, and 466 cm^{-1} for Si-O bending. A closer examination of Figure 9(c) suggests that the reinforcement of PP with OMMT alters the shape and position of the infrared absorption bands of PP and OMMT. The broad peak at 1,047 cm^{-1} (spectrum (b)) spanned from about 1,110 to 1,000 cm^{-1} corresponds to the deformation stretching of Si-O-Si bond in the tetrahedral silicate plane and shows a shape deformation of the peaks (spectra (c) and (d)). The absorption bands of PP between the peaks at 999 and 972 cm^{-1} corresponding to the deformation of tertiary methyl skeletal which is highlighted with a full line box in Figure 9 were modified after the reinforcement with OMMT. The change of the bands at 1,047 cm^{-1} along with the 999 and 972 cm^{-1} indicated that a strong interaction between the PP matrix and OMMT had taken place, the results of which are in good agreement with those from Deshmane et al.[19] The addition of the aryl amide nucleator to PP/PP-*g*-MA/OMMT creates the specific absorption peaks of aryl amide at 1,628 and 1,548 cm^{-1} in Figure 9(d) while it does not impose any change in other peaks compared with Figure 9(c). This FTIR spectrum indicates that aryl amide does not affect the interaction between the PP matrix and OMMT in PP/PP-*g*-MA/OMMT nanocomposites.

CONCLUSIONS

The present research indicated that the addition of aryl amide as a β-nucleating agent improved the impact property of neat polypropylene by approximately 136% with only a slight loss in the flexural modulus. The Izod impact strength of the PP/PP-*g*-MA/OMMT nanocomposite did not increase further by the addition of the nucleating agent. However, the PP/PP-*g*-MA/OMMT nanocomposite system of the work gained both a higher impact strength (50%) and flexural modulus (30%) compared with that of the neat PP. The crystallization peak temperature of the PP/PP-*g*-MA/OMMT nanocomposite was slightly higher with a T_{cp} at 116°C, whereas the effect of β-nucleation increased the crystallization peak temperature of the PP/PP-*g*-MA/OMMT/aryl amide to 128°C, which is of great advantage in commercial scale mold processing of the nanocomposite with, for example, the resulting lower cycle times. Other positive effects of β-nucleation of the PP nanocomposites were a slight reduction in density and an improvement in the very low elongation at break by some 207% at 92% beta nucleation. The beta nucleation of PP nanocomposites can thus be optimized to obtain a better balance between the thermal and mechanical properties.

The authors thank the Program of Petrochemistry and Polymer Science, Faculty of Science, Chulalongkorn University, and IRPC Public Company Limited for providing research facility, research materials, and financial support for characterization. Further, the authors thank the Department of Imaging and Printing Technology for providing facilities for research follow-up. Many thanks go to the PCU for language corrections.

References

1. Lee, H. S.; Fasulo, P. D.; Rogers, W. R.; Donald R. P. Polymer 2005, 46, 11673.
2. Harutun, G. K. Handbook of Polypropylene and Polypropylene Composites, 2nd ed.; Michigan: Marcel Dekker, 2003; p 707.
3. Sperling, L. H. Introduction to Physical Polymer Science, 4th ed.; New Jersey: John Wiley & Sons, 2006; p 687.
4. Lertwimolnun, W.; Vergnes, B. Polymer 2005, 46, 3462.
5. Jayaraman, K.; Kumar, S. Polypropylene Layered Silicate Nanocomposites; Michigan: Michigan State University, Woodhead Publishing, 2006; p130.
6. Wang, Y.; Chen, F. B.; Li, Y. C.; Wu, K. C. Compos B 2004, 35, 111.
7. Kim, D. H.; Fasulo, P. D.; Rodgers, W. R.; Donald, R. P. Polymer 2007, 48, 5308.
8. Moore, E. P. Polypropylene Handbook; Ohio: Hanser Publisher, 1996; p 113.
9. Michler, G. H.; Balta-Calleja, F. J. Mechanical Properties of Polymers Based on Nanostructure and Morphology; Boca Raton, Madrid: CRC Press, Taylor & Francis Group, 2005; p 245.
10. Lotz, B. Polymer 1998, 39, 4561.
11. Trongtosak, K.; Supapol, P.; Tantayanon, S. Polym Test 2004, 23, 533.
12. Zhang, P.; Liu, X.; Li, Y. Mater Sci Eng A 2006, 434, 310.
13. Cho, K.; Seheb, D. N.; Choi, J.; Yang, H. Polymer 2001, 43, 1407.
14. Varga, J.; Mudra, I.; Ehrenstein, G. W. J Appl Polym Sci 1999, 74, 2357.
15. Li, J. X.; Cheung, W. L. Polymer 1998, 40, 2085.
16. Li, J. X.; Cheung, W. L.; Jia, D. Polymer 1999, 40, 1219.
17. Nayak, P. S.; Singh, B. K. Bull Mater Sci 2007, 30, 235.
18. Olley, R.; Bassett, D. C.; Hine, P. J.; Ward, I. M. J Mater Sci 1993, 28, 1107.
19. Deshmane, C.; Yuan, Q.; Perkins, R. S.; Misra, R. D. K. Mater Sci Eng A 2007, 458, 150.
20. LeBaron, P. C.; Wang, Z.; Pinnavaia, T. J. Appl Clay Sci 1999, 15(1-2), 11.
21. Turner-Jones, A.; Aizlewood, J. M.; Beckett, D. R. Makromol Chem 1964, 75, 134.
22. Solomon, M. J.; Almusallam, A. S.; Seefeldt, K. F.; Somwangthanaroj, A.; Varadan, P. Macromolecules 2001, 34, 1864.
23. Rohlmann, C. O.; Failla, M. D.; Quinzani, L. M. Polymer 2006, 47, 7795.
24. Wang, K.; Liang, S.; Zhao, P.; Cheng, Q.; Tan, H.; Du, R.; Zhang, Q.; Fu, Q. Acta Mater 2007, 55, 3143.
25. Dong, Y.; Bhattacharyya, D. Mater Sci Eng A 2010, 527, 1617.
26. Lew, C.Y.; Murphy, W. R.; McNally, G. M.; Abe, K.; Yanai, S. ANTEC 2005,1449.